Supporting Information

Ultrahigh Reversible Lithium Storage of Hierarchical Porous Co-Mo Oxides via Graphene Encapsulation and Hydrothermal S-Doping

Jiatao Chen[a,b], Kongjun Zhu[a,*], Penghua Liang[a,b], Meng Wu[a,b],Yu Rao[a,b], Hongjuan Zheng[a], Jinsong Liu[b], Kang Yan[a] and Jing Wang[a]

[a] State Key Laboratory of Mechanics and Control of Mechanical Structures, College of Aerospace Engineering, Nanjing University of Aeronautics and Astronautics, Nanjing, 210016, China.

[b] College of Materials Science and Technology, Nanjing University of Aeronautics and Astronautics, Nanjing, 210016, China.

[*]Corresponding author: kjzhu@nuaa.edu.cn (Kongjun Zhu).

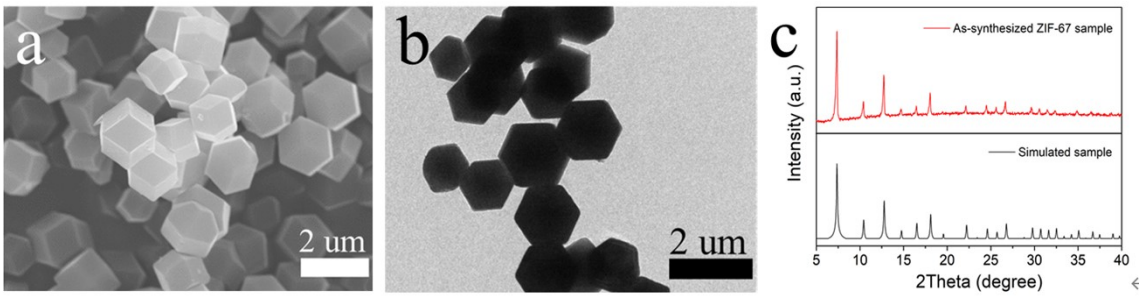

Figure S1. a) SEM image, b) TEM image and c) XRD patterns of ZIF-67 crystals

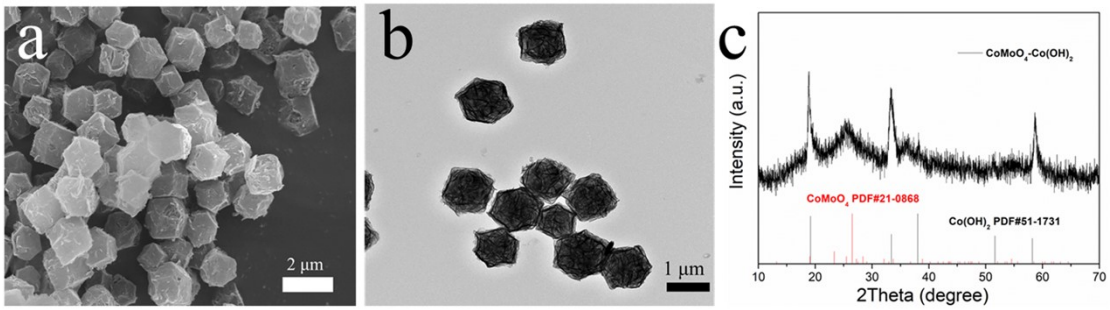

Figure S2. a) SEM image, b) TEM image and c) XRD pattern of $CoMoO_4$-$Co(OH)_2$ NPs

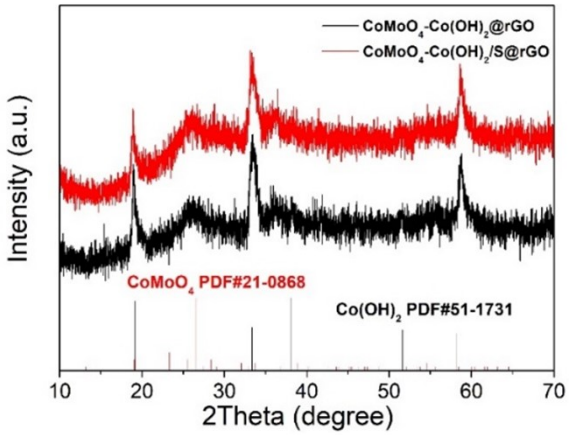

Figure S3. XRD patterns of $CoMoO_4$-$Co(OH)_2$@rGO and $CoMoO_4$-$Co(OH)_2$/S@rGO NPs

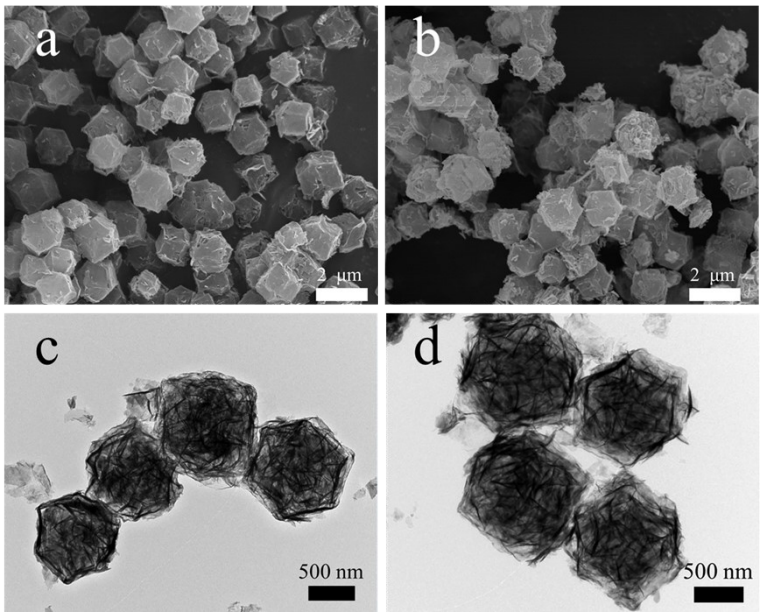

Figure S4. a) SEM image of $CoMoO_4$-CoO/S@rGO. b) SEM image of $CoMoO_4$-CoO@rGO. c) TEM image of $CoMoO_4$-CoO/S@rGO. d) TEM image of $CoMoO_4$-CoO@rGO.

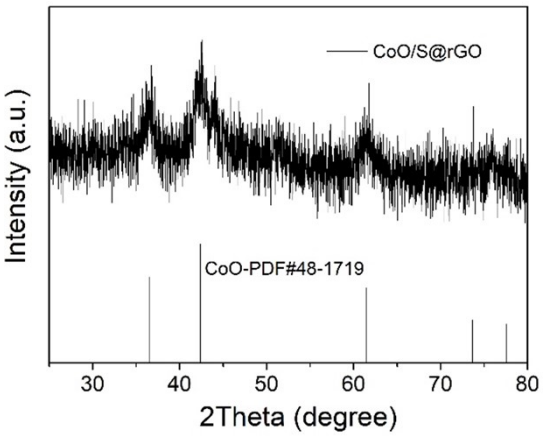

Figure S5. XRD pattern of CoO/S@rGO.

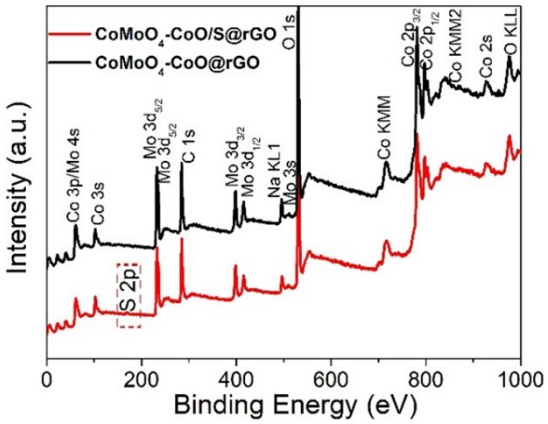

Figure S6. XPS survey spectra of $CoMoO_4$-CoO/S@rGO and $CoMoO_4$-CoO@rGO NPs.

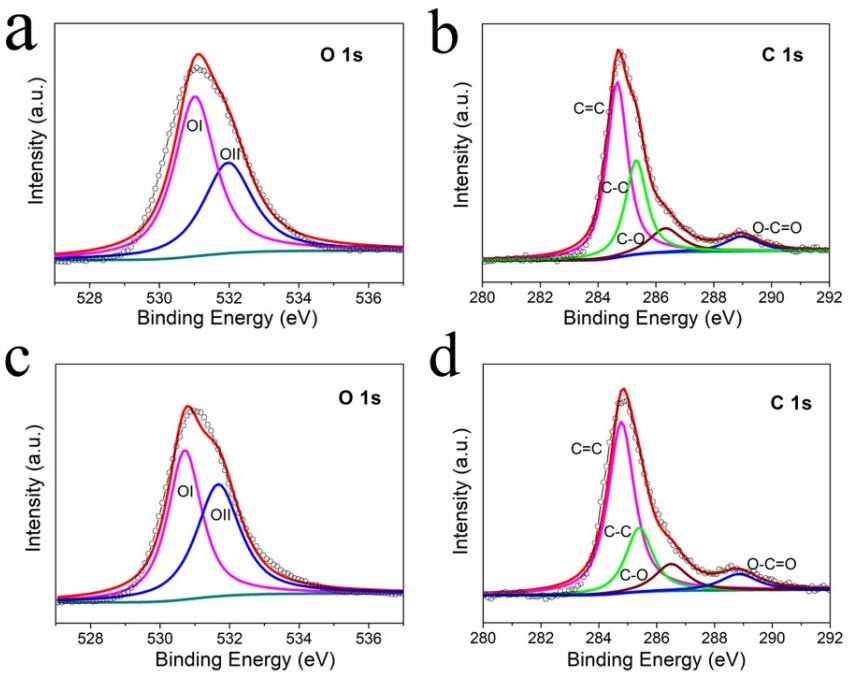

Figure S7. High-resolution a) O 1s, b) C 1s XPS spectra of $CoMoO_4$-CoO/S@rGO. High-resolution c) O 1s, b) C 1s XPS spectra of $CoMoO_4$-CoO@rGO.

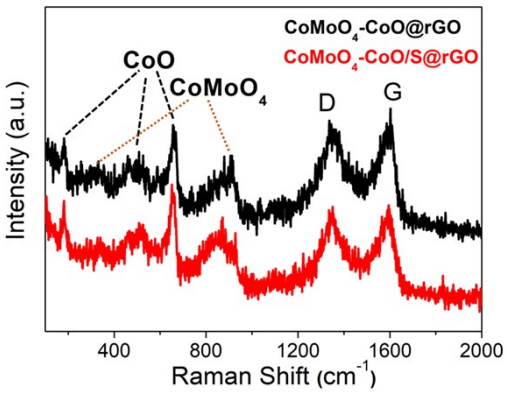

Figure S8. Raman spectra of $CoMoO_4$-CoO/S@rGO and $CoMoO_4$-CoO@rGO NPs.

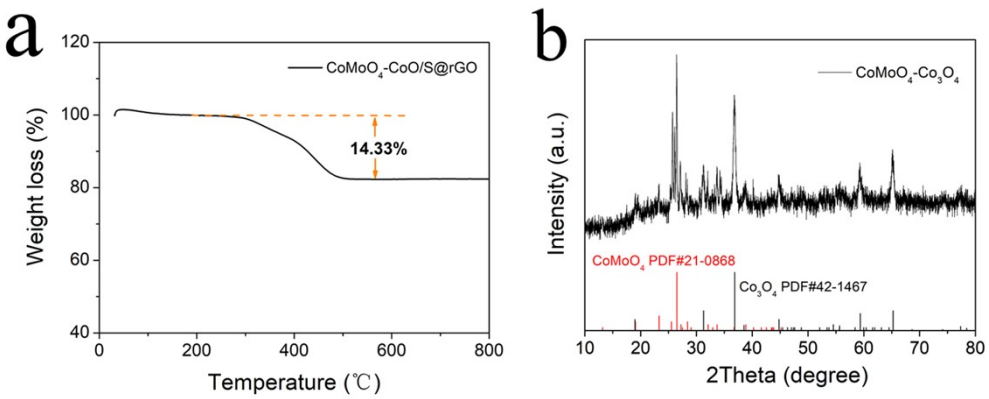

Figure S9. a) TGA curve of $CoMoO_4$-CoO/S@rGO NPs under air atmosphere. b) XRD pattern of powders obtained after TG test.

From room temperature to 200 ℃, the weight loss could due to the release of H_2O and the little weight increase at the beginning could attribute to dry powders absorbing moisture from the air. The main weight variation (~14.33 wt%) from 200 ℃ to 600 ℃ originates from the combustion of the rGO and the oxidation of CoO to Co_3O_4, which can be seen from the XRD pattern of powders obtained after TG test (Figure S10b). From Table S1, we can roughly estimate the proportion of CoO in $CoMoO_4$-CoO/S is ~65% according to the Mo and Co atomic content. Thus, the weight increase from CoO to Co_3O_4 is ~2.76 wt% ($\frac{65\% \times 74.9}{65\% \times 74.9 + 35\% \times 218.9} \times 7.1\%$). Therefore, the rGO content in the $CoMoO_4$-CoO/S@rGO NPs is around 17.09 %.

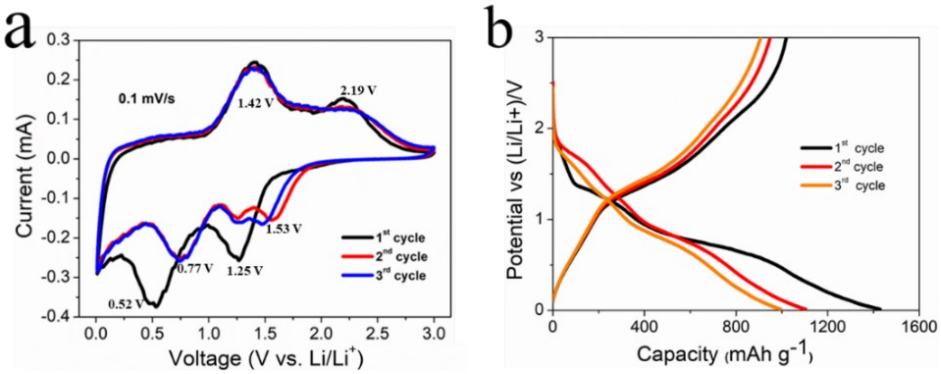

Figure S10. a) The first three cycles of CV curves at 0.1 mV s^{-1} of $CoMoO_4$-CoO@rGO electrode. b) The first three charge/discharge curves of $CoMoO_4$-CoO@rGO electrode at 0.5 A g^{-1}.

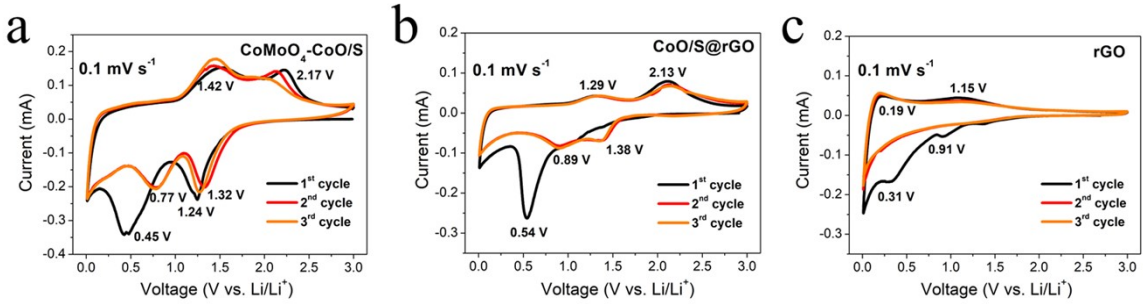

Figure S11. The first three cycles of CV curves at 0.1 mV s^{-1} of a) the $CoMoO_4$-CoO/S electrode, b) CoO/S@rGO electrode, and c) rGO electrode.

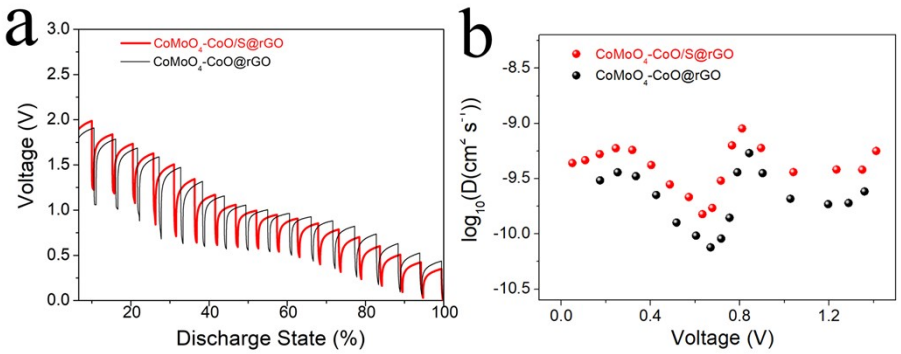

Figure S12. a) Discharge state curves of GITT measurement for $CoMoO_4$-CoO/S@rGO and $CoMoO_4$-CoO@rGO electrodes at 0.5 A g^{-1}. b) The D_{Li^+} of $CoMoO_4$-CoO/S@rGO and $CoMoO_4$-CoO@rGO electrodes during the discharge process at 0.5 A g^{-1}.

The Li-ion diffusion coefficients of $CoMoO_4$-CoO/S@rGO and $CoMoO_4$-CoO@rGO electrodes can be measured according to the following Equation (1)

$$D_{Li^+} = \frac{4L^2}{\pi\tau}\left(\frac{\Delta E_S}{\Delta E_\tau}\right)^2 \quad (1)$$

where L and τ are the thickness of the electrodes (cm) and the duration of the current pulse (s), respectively. ΔE_s is the change in steady-state voltage (V) for a single-step GITT measurement, and ΔE_τ is the voltage change (V) during one discharge pulse regardless of IR drop.

Table S1. Elemental quantification of $CoMoO_4$-CoO/S@rGO

	Co (wt. %)	Mo (wt. %)	S (wt. %)
$CoMoO_4$-CoO/S@rGO	21.43	7.4	0.35

Table S2. Comparison of specific capacity of $CoMoO_4$-CoO/S@rGO electrode with some CoO-based materials

Materials	Current density (A g^{-1})	Cycle number	Specific capacity (mAh g^{-1})	Ref.
$CoMoO_4$-CoO/S@rGO	0.5	150	1103	This work
	2.0	300	700	
CoO-NCNTs	0.5	2000	583	1
CoO@C	0.5	300	890	2
CoO/N, S-C	1.0	500	805	3
CoO/C YSNSs	1.0	1000	672	4
CoO-graphene hydrogel	0.1	100	1010	5
CoO/$Co_2Mo_3O_8$@MXene	2.0	1200	545	6
CoC_2O_4@CoO/Co	0.2	200	837	7
Co_3O_4/CoO/Co foam	0.1	50	989	8
CoO/$MnCo_2O_{4.5}$	1.0	120	657	9
CoO/$CoFe_2O_4$/EG	1.0	700	890	10

1 Y. Pang, S. Chen, C. Xiao, S. Ma and S. Ding, *J. Mater. Chem. A*, 2019, **7**, 4126-4133.

2 F. Wu, S. Zhang, B. Xi, Z. Feng, D. Sun, X. Ma, J. Zhang, J. Feng and S. Xiong, *Adv. Energy Mater.*, 2018, **8**.

3 F. Wang, H.-Y. Zhuo, X. Han, W.-M. Chen and D. Sun, *J. Mater. Chem. A*, 2017, **5**, 22964-22969.

4 S. Wang, J. Teng, Y. Xie, Z.-W. Wei, Y. Fan, J.-J. Jiang, H.-P. Wang, H. Liu, D. Wang and C.-Y. Su, *J. Mater. Chem. A*, 2019, **7**, 4036-4046.

5 G. Binitha, A. G. Ashish, D. Ramasubramonian, P. Manikandan and M. M. Shaijumon, *Adv. Mater. Interfaces*, 2016, **3**.

6 X. Zhao, H. Xu, Z. Hui, Y. Sun, C. Yu, J. Xue, R. Zhou, L. Wang, H. Dai, Y. Zhao, J. Yang, J. Zhou, Q. Chen, G. Sun and W. Huang, *Small*, 2019, **15**, e1904255.

7 Z. He, L.-a. Huang, J. Guo, S.-e. Pei, H. Shao and J. Wang, *Energy Storage Mater.*, 2020, **24**, 362-372.

8 H. Park, K. Kim, K. Jeong, J. S. Kang, H.-H. Cho, B. Thirumalraj, Y.-E. Sung, H. N. Han, J.-H. Kim, D. C. Dunand and H. Choe, *Appl. Surf. Sci.*, 2020, **525**.

9 L. Ni, W. Tang, X. Liu, N. Zhang, J. Wang, S. Liang, R. Ma and G. Qiu, *Dalton Trans.*, 2018, **47**, 3775-3784.

10 L. Ye, C. Wang, L. Cao, H. Xiao, J. Zhang, B. Zhang and X. Ou, *Green Energy Environ.*, 2021, **6**, 725-733.